AIAA SciTech Forum
4-8 January 2016, San Diego, California, USA
54th AIAA Aerospace Sciences Meeting

10.2514/6.2016-1395

Large eddy simulation of flame stabilization in a multi-jet burner using a non-adiabatic flamelet approach

Yihao Tang* Malik Hassanaly† Heeseok Koo‡ Venkat Raman§
University of Michigan, Ann Arbor, Michigan, 48109, U.S.A.

In this study, H2/air premixed combustion in a recirculation-stabilized multi-burner combustor is simulated with LES and non-adiabatic flamelet method. The combustor is operated at 8 bar pressure under very lean conditions ($\phi = 0.33$). It is found that the high-velocity jet creates a large recirculation zone that allows the flame to be stabilized inside the combustor. The simulations predict the jet structure and recirculation zone well, but show quantitative differences. In particular, the jet length is shorter in the simulations. It is postulated that this is due to increased shear from a recirculating flow that is stronger than in the experiments. Heat-loss to the walls weakens the recirculation zone and further decreases the core jet length while pushing the flame zone further downstream. Furthermore, higher heat release appears to broaden the reaction zone by significantly reducing reaction rates across the entire domain.

I. Introduction

Environmental concerns leading to increasingly stringent emissions regulations have created the need for extremely low emission gas turbines. In the context of stationary gas turbines that predominantly operate in the premixed mode, the trade-off between low-NOx design and combustor stability remains a critical issue. In particular, low equivalence ratios are used to reduce the operating temperature, but this leads to stability issues. Additionally, the push towards higher operating pressures increases firing temperature, which also increases production of NOx. Several strategies including fuel staging have been proposed as a solution. One approach to stabilization, which lends from the flameless oxidation or FLOX®[1] technology, is the use of exhaust gas recirculation to bring down the temperature gain from heat release. The focus of this work is to understand the flow inside a model combustor that uses large recirculation to stabilize lean premixed combustion.

Figure 1 shows a premixed combustor[2] with and without a central swirl-stabilized pilot stage. As seen, the circular ring of inlet holes around the center of the burner issues high momentum jets with premixed fuel/air mixture. Due to the non-axisymmetric configuration of these jets, heat release and subsequent wall interactions lead to the jets bending towards the center. This process creates large recirculation zones near the center as well as near the walls that aid flame stabilization. The high velocity of the inflow jets prevents flame flashback, but the low recirculation zones allow sufficient heating of fuel-air mixture to stabilize the combustion process. The interaction of multiple jet flames, the heat loss near the walls, and the response of the recirculation zone to this heat loss are the main considerations in the design of a stable combustor.

The recirculation zone inside the combustor is mainly driven by the jet breakdown and its trajectory as it moves towards a constricted outflow. For this purpose, a 3-jet system was experimentally studied by the German Aerospace Center (DLR).[3] This configuration isolates the interaction of multiple jets with a recirculation zone, and is well-suited for validating and analyzing models. With this background, the study here develops a robust large eddy simulation (LES) platform based on the open source OpenFOAM approach,

*Graduate Student, Department of Aerospace Engineering, yhtang@umich.edu,AIAA Student Member.
†Graduate Student, Department of Aerospace Engineering, malik.hassanaly@gmail.com, AIAA Student Member.
‡Postdoctoral Scholar, Department of Aerospace Engineering, heeseokkoo@gmail.com, AIAA Member.
§Associate Professor, Department of Aerospace Engineering, ramanvr@umich.edu, AIAA Senior Member.

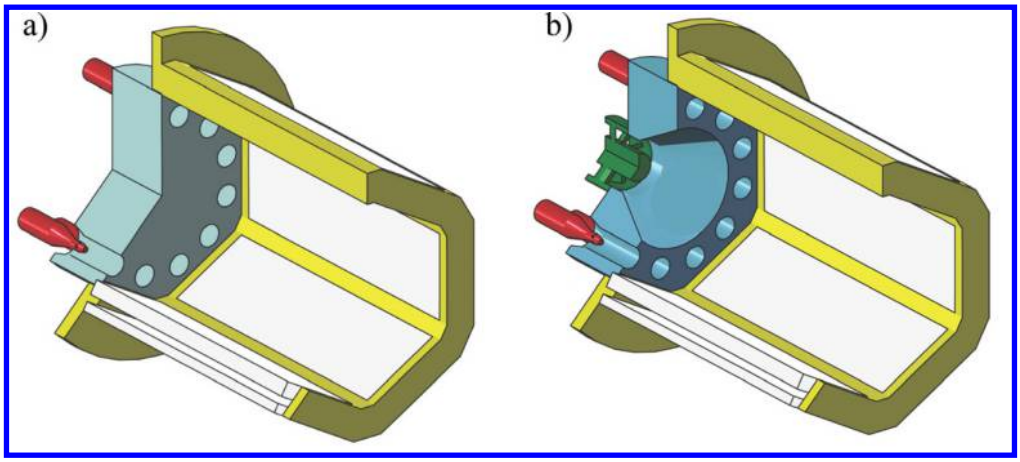

Figure 1. General layouts of FLOX® gas turbine combustors with: a) single-stage configuration b) piloted system.

incorporates a new non-adiabatic flamelet approach for simulating such recirculating premixed flames, and validates using DLR experimental configurations. The rest of the text is laid out as follows. First, the computational modeling of such premixed flames is discussed. The simulation of the DLR experimental configurations is then presented, and the paper finishes with conclusions.

II. Computational modeling of premixed flames with heat loss

The main flow configuration consists here of a fully premixed fuel/air inflow that is stabilized through recirculation of products. For this purpose, the LES approach is combined with a non-adiabatic flamelet model. In the sections below, the LES approach is discussed first, followed by the non-adiabatic flamelet approach.

II.A. LES approach for unstructured mesh based geometries

The governing equations of fluid flow (i.e., mass, momentum, energy, and species transport) are filtered using a low-pass filter to obtain the LES transport equations. A low-Mach number assumption is used to solve the gas phase, where the energy equation is decoupled from the momentum equation. In the case of an adiabatic flow, the energy equation is redundant, but when heat loss is important, a transport equation for some form of enthalpy needs to be solved, as discussed in the combustion modeling section below. The solution of such low-Mach number systems has been widely studied[4–8] and is not repeated here. However, it is important to note that the implementation of such solvers in a collocated mesh system requires special considerations.[9,10] In particular, LES equations are designed to conserve momentum and other variables that are directly solved for, but are required to preserve other quantities such as kinetic energy that are not directly evolved. This secondary conservation is not automatic, and is obtained using special choice of discretization operators.

The LES equations for momentum, energy and scalar fields are implemented in OpenFOAM.[11] OpenFOAM is an operator-based C++ codebase for solving partial differential equations which has been applied to model a number of combustion systems.[12–14] However, the baseline codebase was substantially modified to ensure accurate evolution of the LES equations. In structured-grid solvers that use staggered positioning of velocity and pressure variables, secondary conservation can be ensured by specific choice of divergence and gradient operators.[10,15,16] In fully unstructured mesh solvers, such as the one used here, a collocated variable approach is used, which prevents exact secondary conservation of kinetic energy. In general, minimally dissipative schemes are sought in order to reduce the effect of kinetic energy loss on flow evolution. Here, the variable density scheme of Morinishi[17] is used. The fluxes at the cell faces are computed using mid-point interpolation scheme. The governing equations are solved using a semi-implicit approximation that is second-order in time. This approach directly relates energy conservation to temporal convergence of the numerical scheme. To ensure second-order accuracy, a Pressure-Implicit Second Order (PISO) scheme is used[18] with at least two inner iterations. This solver was found to provide equal rate of energy dissi-

pation as compared to other staggered-mesh unstructured flow solvers.[13] This new variable density solver, umFlameletFoam[13,14,19] is used for all the simulations discussed below.

II.B. Non-adiabatic flamelet model for premixed combustion

In a reacting system with detailed chemistry mechanism, besides solving conservation equations of mass, momentum and energy, extra equations for each species is solved as:

$$\frac{\partial \overline{\rho}\tilde{\phi}_i}{\partial t} + \frac{\partial \overline{\rho}\tilde{\phi}_i \tilde{u}_j}{\partial x_j} = \frac{\partial}{\partial x_j}\left(\tilde{D} + D_T\right)\frac{\partial \tilde{\phi}_i}{\partial x_j} + \overline{\rho}\tilde{S}_{\phi_i}, \tag{1}$$

where $\tilde{\phi}_i$ corresponds to i^{th} species, $\widetilde{u}_j$ denotes a velocity component. D and D_T represent molecular and turbulent diffusivity respectively, and the filtered chemical source term $\tilde{S}_{\phi_i}$ is unclosed. Given the non-linearity of this source term and the complexity of typical chemical reactions, the computational resources for this calculation rises rapidly. In the interest of cost reduction, a computationally efficient alternative - flamelet progress variable approach[20–22] - is used to determine the local thermochemical composition. In the adiabatic version, this model assumes a flame thin enough that turbulent eddies do not penetrate, serving only to contort the front. Under this assumption, the flame appears to be locally laminar. A single transported variable serving only to mark the progress of combustion is necessary. The thermochemical vector is then mapped to this reaction progress variable, and transport equations for species and energy are replaced with the following

$$\frac{\partial \overline{\rho}\tilde{C}}{\partial t} + \frac{\partial \overline{\rho}\tilde{C}\tilde{u}_j}{\partial x_j} = \frac{\partial}{\partial x_j}\left(\tilde{D} + D_T\right)\frac{\partial \tilde{C}}{\partial x_j} + \overline{\rho}\tilde{S}_C \tag{2}$$

resulting in only a single unclosed term. In principle, C can be any linear combination of species mass fractions, which obeys the rule $\nabla C \neq 0$ through the flame front. And in this case C is defined using species mass fractions,

$$C = Y_{H_2} \tag{3}$$

for hydrogen reaction. The filtered source term, $\tilde{S}_C$, as well as the filtered density, molecular viscosity, and temperature are read from a flamelet lookup table assembled before the simulation. The table is obtained by solving a 1-D laminar flame with detailed chemistry mechanism. An example of the resulting table is shown in Fig. 2.

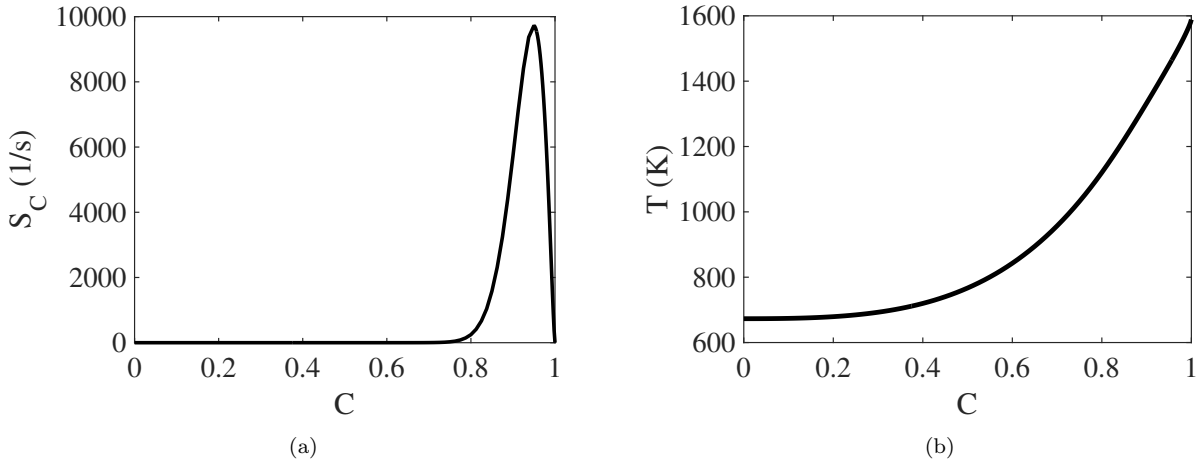

Figure 2. Plot of: a) source of C b) temperature vs. C.

So far, the progress variable C is the only variable allowed to vary freely in the flamelet table, and enthalpy is automatically conserved in the flamelet solution, resulting in an adiabatic system. To include heat loss effects, an additional controlling variable related to enthalpy is added to the original adiabatic flamelet table, resulting in a non-adiabatic flamelet approach. In the following subsections, three major

aspects of the non-adiabatic flamelet approach applied here is explained, including how the flamelet energy equation is modified to include heat loss, how tabulation for low enthalpy region is applied, and how the resulting non-adiabatic table is coupled with CFD code.

II.B.1. Non-adiabatic flamelet equation

Typically, there are two ways to introduce heat loss in the flamelet model. The first approach is to change the total enthalpy of the flow either by decreasing the unburnt fuel/air temperature[23] or by changing the mass flow rate of a burner stabilized flame.[24] The second approach introduces a sink term in the flamelet equations, and is followed here. This approach allows for a more local control of heat loss rather than the first approach. More importantly, the rate of heat loss can be parameterized using physically-relevant variables. For instance, radiation heat losses are accounted for by using a power law for temperature.[25] Here, heat loss is through transfer to the wall, which can be modeled using a wall-conduction term based on an imposed temperature. The flamelet equation for energy is modified as

$$\rho_0 S_L \frac{dh_s(x)}{dx} = \frac{d}{dx}\left(\lambda \frac{dT}{dx}\right) + \sum_{i=1}^{n} \rho h_{s,i}(x) D_i \frac{d\phi_i(x)}{dx} + \omega_{h_s}(x) + S_d(x), \tag{4}$$

where ρ_0 is the unburnt density, h_s is the sensible enthalpy, $\omega_{h_s}(x)$ is the volumetric source term due to chemical reaction, D_i is the molecular diffusion coefficient for species i, and ϕ_i is the mass fraction of species i. The sink term S_d is expressed as a Fourier conduction term:

$$S_d(x) = -\lambda \frac{T(x) - T_w}{\delta^2}, \tag{5}$$

where T_w is the imposed wall temperature, and δ is a characteristic length scale over which the heat loss occurs. This latter term is a variable and can be changed to generate a family of flamelet solutions which span a range of enthalpy losses experienced by the actual flow configuration. This equation is solved using the FlameMaster code.[26]

II.B.2. Interpolation to lower enthalpy

The non-adiabatic flamelet solutions introduced above do not cover the entire region of composition space that they alone cannot cover the entire total enthalpy space. For instance, when the heat loss is large (δ is small), the flamelet solutions lead to the quenched branch. Consequently, a large region of phase space is not captured by the flamelet solutions. However, this region may be accessed in a practical flow, especially when the burn product is cooled in the near-wall region. To cover the full enthalpy space, an interpolation procedure is developed here.

The main idea is based on the model of Trisjono and Pitsch,[27] where a flamelet model with heat loss is obtained by rescaling around a base table without solving anymore non-adiabatic flamelet equations. Here, a similar approach is used for the interpolation in zones with large heat loss. To start with, the mixture enthalpy is defined based on the species mass fractions and temperature as follows:

$$h = \sum_{i=1}^{n} \phi_i h_i(T) \tag{6}$$

with $h_i(T)$ further expressed as a NASA polynomial.[28]

In the quenched zone with no flamelet solution, the species composition is assumed to be frozen as a reference value, where the reference value is determined based on the non-adiabatic flamelet solution with the lowest available enthalpy and the same progress variable value. Then, the temperature can be obtained from Eq. 6 for a given h and $\phi_i, i = 1, \cdots, n$. Based on this temperature, the gas density and other thermochemical properties can be determined. Finally, the progress variable source term is obtained by using a rescaled Arrhenius law as

$$S_c = S_{cr} \exp\left(-\frac{E_a}{R}\left(\frac{1}{T} - \frac{1}{T_{ref}}\right)\right), \tag{7}$$

where subscript r refers to the reference state and activation energy E_a determined from a 1-step reaction mechanism.[29] This process is carried out for all combinations of h, C for which no flamelet solution exists.

II.B.3. Integration of non-adiabatic flamelet approach into CFD code

With non-adiabatic effects included, an energy transport equation needs to be solved. In order to ensure consistency in the limit where there are no heat losses, a modified heat loss parameter is used instead of directly solving the enthalpy itself.[25] This parameter H is defined as

$$H = h - h_{Ad}, \tag{8}$$

where h is the total enthalpy, and h_{Ad} is the adiabatic total enthalpy under a fictional adiabatic situation with the same C value. Since H is by definition equal to zero for adiabatic situations, it simplifies inlet boundary condition setup.

The transport equation of the heat loss parameter H is derived from the transport equations of h and h_{Ad}. After neglecting the species diffusion, volumetric forces, pressure and viscous contribution, and radiation terms, the energy equations can be written as

$$\frac{\partial \overline{\rho}\tilde{h}}{\partial t} + \frac{\partial \overline{\rho}\widetilde{u}_j\tilde{h}}{\partial x_j} = \frac{\partial}{\partial x_j}\left(\frac{\mu_T}{Pr}\frac{\partial \tilde{h}}{\partial x_j}\right) + \frac{\partial}{\partial x_j}\left(\tilde{\lambda}\frac{\partial \tilde{T}}{\partial x_j}\right) \tag{9}$$

and

$$\frac{\partial \overline{\rho}_{Ad}\tilde{h}_{Ad}}{\partial t} + \frac{\partial \overline{\rho}_{Ad}\widetilde{u}_{j,Ad}\tilde{h}_{Ad}}{\partial x_j} = \frac{\partial}{\partial x_j}\left(\frac{\mu_{T,Ad}}{Pr}\frac{\partial \tilde{h}_{Ad}}{\partial x_j}\right) + \frac{\partial}{\partial x_j}\left(\tilde{\lambda}_{Ad}\frac{\partial \tilde{T}_{Ad}}{\partial x_j}\right), \tag{10}$$

where all the adiabatic properties are defined at the same conditions for which h_{Ad} is evaluated. The Prandtl number Pr, defined as the ratio of momentum diffusivity to thermal diffusivity, is set to 1 in this study. By subtracting equation (10) from (9), the transport equation of heat loss parameter H is obtained as

$$\frac{\partial \overline{\rho}\tilde{H}}{\partial t} + \frac{\partial \overline{\rho}\widetilde{u}_j\tilde{H}}{\partial x_j} = \frac{\partial}{\partial x_j}\left(\frac{\mu_T}{Pr}\frac{\partial \tilde{H}}{\partial x_j}\right) + \frac{\partial}{\partial x_j}\left(\tilde{\lambda}\frac{\partial \tilde{T}}{\partial x_j}\right) - \frac{\partial}{\partial x_j}\left(\tilde{\lambda}_{Ad}\frac{\partial \tilde{T}_{Ad}}{\partial x_j}\right) \tag{11}$$

and currently the terms $\frac{\partial(\overline{\rho}-\overline{\rho}_{Ad})\tilde{h}_{Ad}}{\partial t}$, $\frac{\partial(\overline{\rho}\widetilde{u}_j-\overline{\rho}_{Ad}\widetilde{u}_{j,Ad})\tilde{h}_{Ad}}{\partial x_j}$, and $\frac{\partial}{\partial x_j}\left(\frac{\mu_T-\mu_{T,Ad}}{Pr}\frac{\partial \tilde{h}_{Ad}}{\partial x_j}\right)$ are neglected in this study, by assuming $\rho \approx \rho_{Ad}$, $u \approx u_{Ad}$, and $\mu \approx \mu_{Ad}$.

Equation (11) is the final form of energy equation solved by the CFD code in this paper. A transformation of flamelet table from the total enthalpy h space into the heat loss parameter H space is also applied, resulting in the final form of the non-adiabatic flamelet table having coordinates in the $H - C$ space. Figure 3 shows the reaction progress variable source term in the $H - C$ space.

III. Simulation of DLR experimental configuration

In this section, the computational details for the 3-jet DLR configuration are first provided, which is followed by a discussion of the simulation results.

III.A. Flow configuration and operating conditions

Three flow conditions corresponding to the DLR 3-jet configuration are simulated here. The combustion domain is shown in Fig. 4, and consists of three identical injection nozzles placed assymetrically in the y-direction. The combustor axis is defined as the line parallel to the x-axis through the center of the middle nozzle. The combustor is 320 mm long with a cross-section of 100 mm × 140 mm. The injection nozzles are connected to long serpentine pipes (shown later as part of the computational mesh), and injet well-developed turbulent flow into the domain. The combustion chamber operates at a pressure of 8 bar with low equivalence ratio. The three cases have differing wall temperatures, but correspond to a single DLR experiment. In the experiment, the wall temperatures were only approximately measured, and is not suitable for the calculations here. Consequently, the wall temperature was varied in the simulations to understand the effect of heat losses on the flow dynamics. Details of the flow conditions are provided in Tab. 1.

As discussed in Sec. II.A, the simulations were carried out using the minimally dissipative OpenFOAM-based LES solver developed at University of Michigan. The computational mesh consisted of a hexahedral element dominated discretization with multiple layers near the wall to resolve boundary layers. In the early stage of study, three meshes of different total cell number (approximate 2, 8, and 16 million) were generated

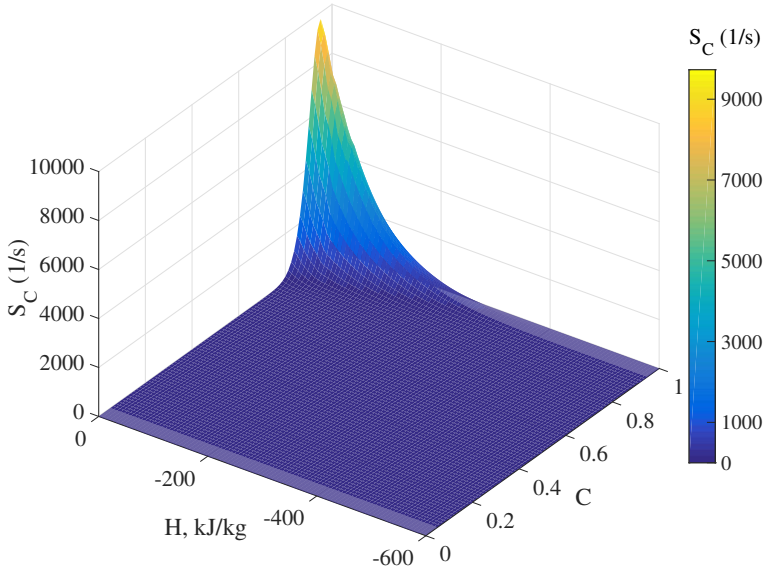

Figure 3. Example of the non-adiabatic table: source of C varying in $H - C$ space.

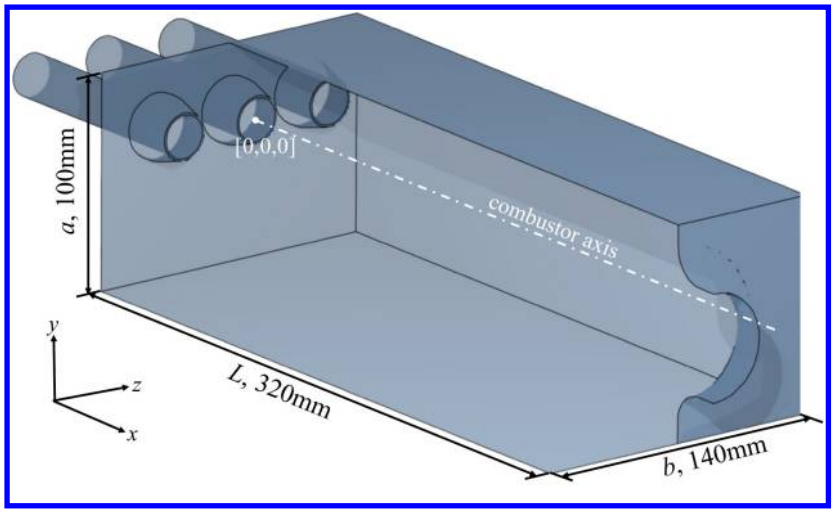

Figure 4. A schematic of the DLR 3-jet combustor, obtained from.[3]

Table 1. Summary of Operating Conditions

Case	Fuel	p, bar	T_u, K	T_w, K	U_{jet}, m/s	ϕ
A	Premixed H_2/Air	8	673	1583	137	0.33
B	Premixed H_2/Air	8	673	1200	137	0.33
C	Premixed H_2/Air	8	673	900	137	0.33

and tested, and it can be seen from Fig. 5 that the mesh of 8 million cells achieves result matching closely with result obtained on the mesh of 16 million cells. Therefore the mesh of 8 million cells is considered to be sufficient to reach mesh convergence, and it is chosen as the computational mesh for later studies. The first layer close to the wall was located at $1.5y^+ \sim 1.8y^+$, where y^+ is the wall unit. Figure 6 gives sample snapshots of the computational mesh used. As seen, the inlet pipes have a complex configuration and are instrumental in developing the boundary layers that reach the chamber. All of the inflow channels are of the same length, with comparable pressure drops. It is also seen that to resolve the inflow boundary layers, a very fine mesh is needed near the walls.

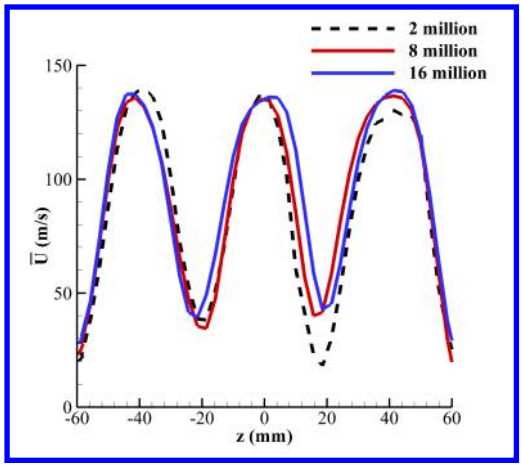

Figure 5. Mean axial velocity obtained from different meshes plotted along z direction at $x = 0$, $y = 0$.

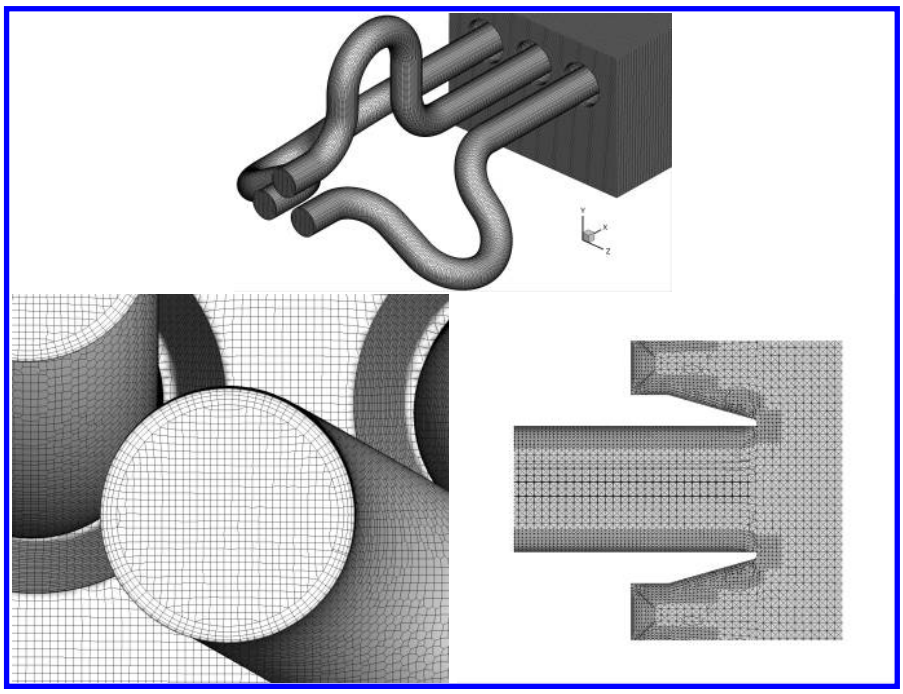

Figure 6. Different views of the computational mesh used for the LES calculations.

III.B. Simulation results

The three test cases (A, B, and C) correspond to different levels of heat loss, with the wall temperature of case A corresponding to the adiabatic temperature for this equivalence ratio. Hence, case A corresponds to

zero heat loss. Figure 7 shows the top-view of the velocity field through the combustor. It is seen that the inflow, although laminar far upstream, quickly transitions to turbulent flow past the bend leading to well-developed turbulent flow issuing through the injection nozzles. However, the jet breaks down downstream of the injection point through interaction with the recirculating flow. Near the outflow, the constriction in the domain leads to flow acceleration. Figure 8 shows comparison of experimental and simulation-based time-averaged axial velocity obtained from the top view. It is seen that the simulations predict the overall jet structure reasonably well. However, the experimental data suggests greater interaction amongst the jets, as evidenced by a smaller low-velocity zone that was created by the gap between the injectors. This suggests increased jet transverse motion, which would indicate some form of jet-flapping instability that is not present in the simulations.

Figure 9 shows centerline velocity profile for both the experiment and the simulation. It is seen that the inflow velocity of the jet is higher than that in the experiments, but the experiment shows a longer jet core along the centerline as compared to the simulations. However, the decay of the jet seems to follow the same slope in both the experiments and simulations, although the simulations predict an earlier start of decay. To understand this effect, it is illustrative to discuss the side view profiles. Figure 10 shows the side view velocity statistics for all three cases as well as the experimental data. It is seen that for the adiabatic case, the jet undergoes strong interactions with the recirculation zone leading to faster decay. In the experiments, the jet does not decay until further downstream, which indicates the the strength of the recirculation is weaker.

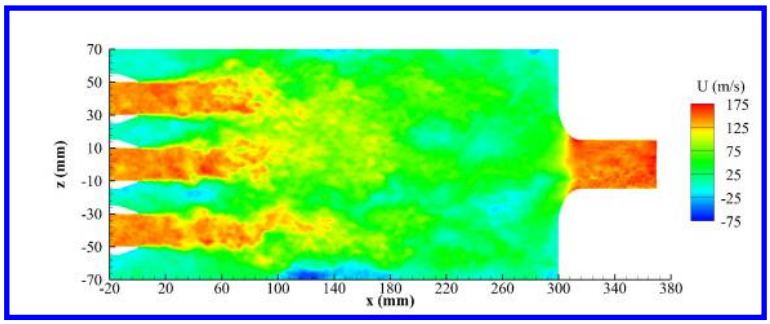

Figure 7. Top-view of instantaneous axial velocity field in case A.

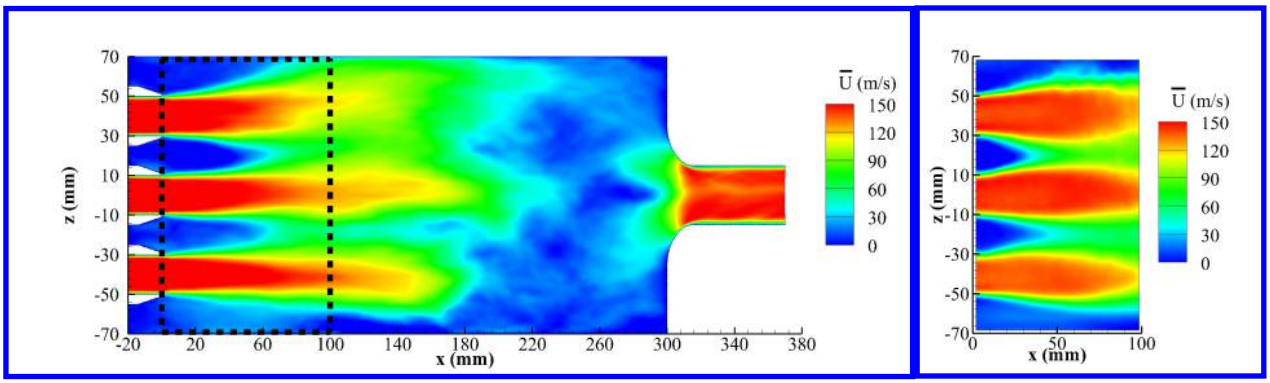

(a) case A (b) PIV

Figure 8. Top-view of mean axial velocity field.

Heat loss will clearly affect the temperature profiles inside the combustor, which will in turn affect the flow field through density changes. To understand the impact of heat loss, cases B and C were simulated. Figure 10 shows the velocity profiles for these cases as well. Interestingly, increase in heat loss reduces the jet length but also reduces the strength of the recirculation zone. Case B shows a large recirculation zone with very high negative values near the lower wall, while case C has a much smaller recirculation zone with higher velocities near the wall. This reduction in recirculation strength can be understood in terms of the temperature profiles. Figure 11 shows the temperature profiles for all three cases. The unburnt core length

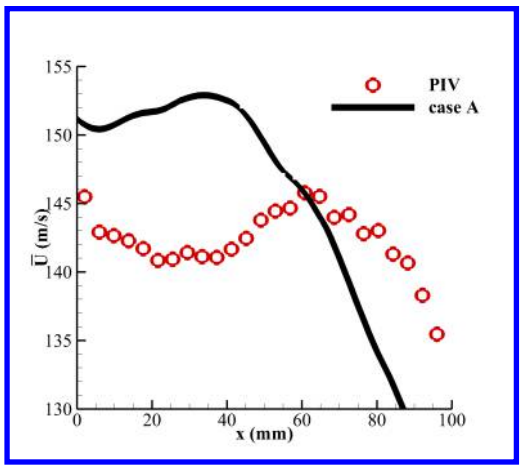

Figure 9. Mean axial velocity plot along combustor axis.

actually increases with increase in heat loss, due to the lower enthalpy of the recirculating gases. This pushes the recirculation zone upstream but also reduces the strength due to the reduced enthalpy. Since the expansion related to the flame front happens farther downstream than in the adiabatic case, the jet core appears weaker with a faster decay. In comparison to the experimental data, the heat loss corresponding to a wall temperature of 1200K appears to provide the correct jet length, yet the recirculation zone is similar to that found in the adiabatic case.

To understand the structure of the flame in this combustor, the instantaneous heat-loss parameter is shown in Fig. 12. Heat loss occurs in four regions of the flow. The near exit top and bottom steps provide a low velocity recirculation region where large residence times increase heat conduction to walls. The top left corner is also a region of low velocity due to the asymmetric jet placement. However, the lower left corner serves as the main heat loss region due to the volume of this zone. Based on the time-averaged velocity contours (Fig. 10), it is seen that the volume of the lower heat loss region decreases with decrease in wall temperature. This indirectly increases the recirculation region near the top right corner, albeit with lower recirculation velocities.

Figure 13 compares scatter plots of frequency of encountering a particular progress variable location in the $H-C$ space. In the higher wall temperature case, only the very high and very low progress variable locations are most often encountered. This implies that heat loss affects mostly the reacted (fully burnt) and unreacted mixture. In other words, the recirculating gases impinge on the jet prior to the flame stabilization region. In the 900K case, a large region within the combustor encounters partially burnt products, which implies a broadening of the flame stabilization region. Furthermore, heat loss is prevalent at all progress variables, implying that the effect of the wall reaches even the core of the jet. However, this reaction broadening would imply a fundamental change in flame structure. Instead of being confined to the thin-flame region, it is now possible that the flame moves into the distributed or broken reaction zones part of the premixed-flame regime diagram.[30] In this case, the ability of the flamelet approach to describe the flame front needs to be re-evaluated.

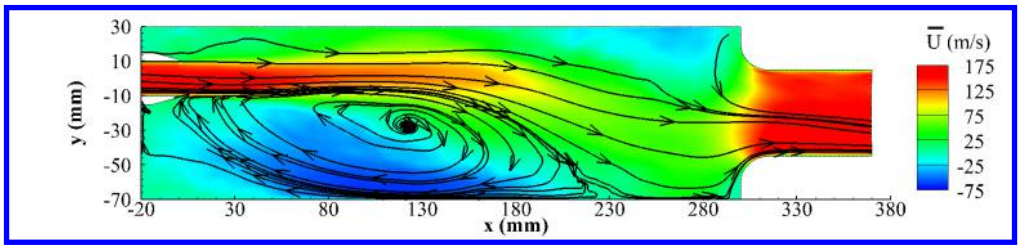

(a) case A

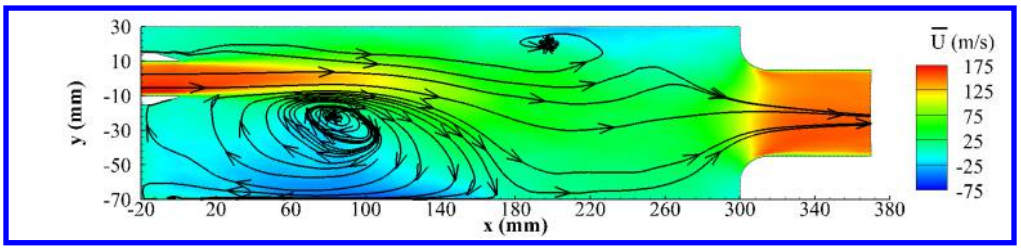

(b) case B

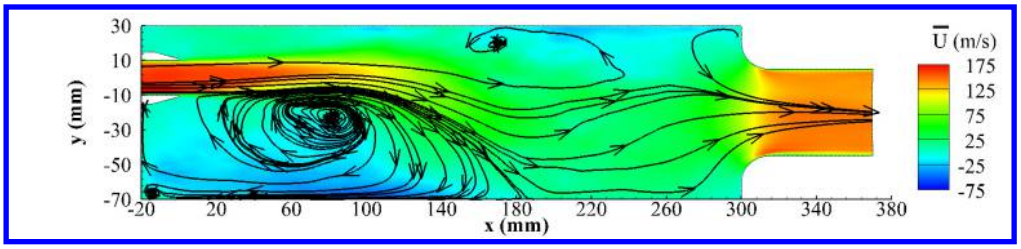

(c) case C

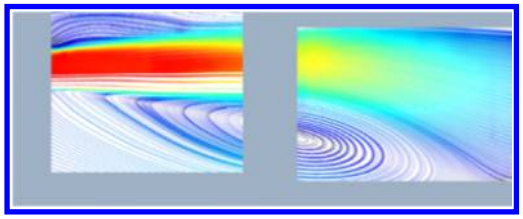

(d) PIV

Figure 10. Side-view of mean axial velocity field plotted with streamline of three cases and PIV streamline result.

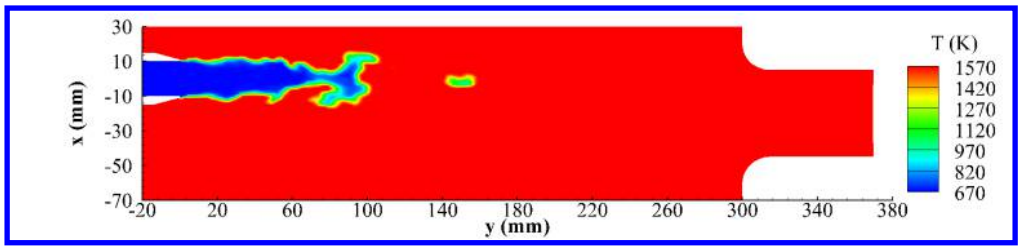

(a) case A

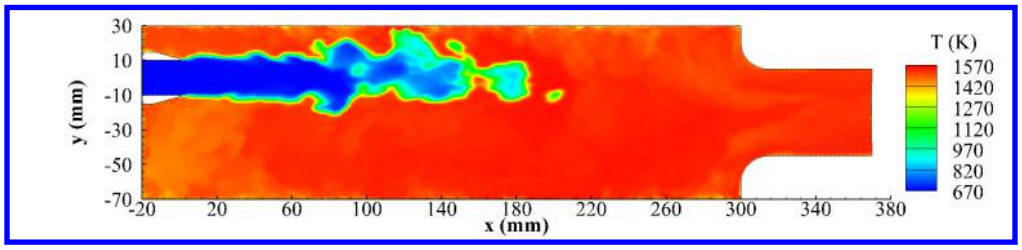

(b) case B

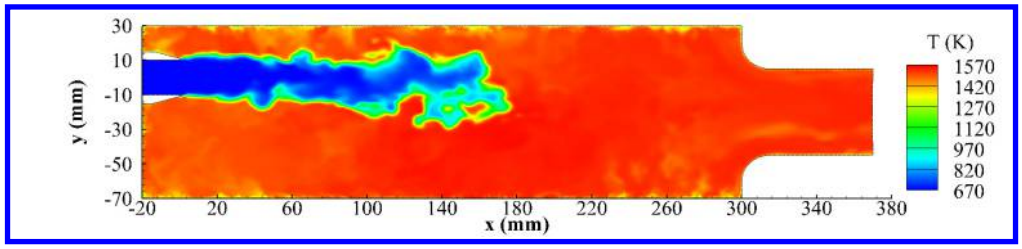

(c) case C

Figure 11. Side-view of instantaneous temperature field.

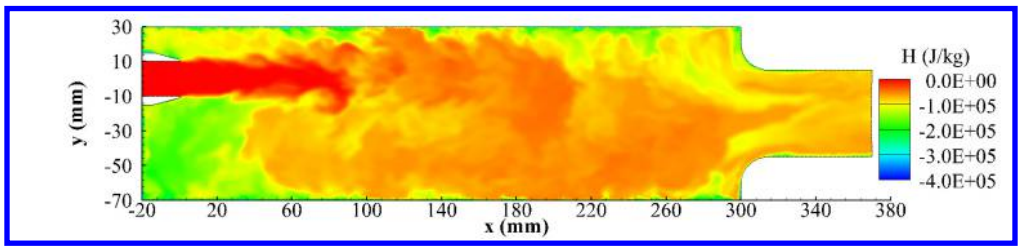

(a) case B

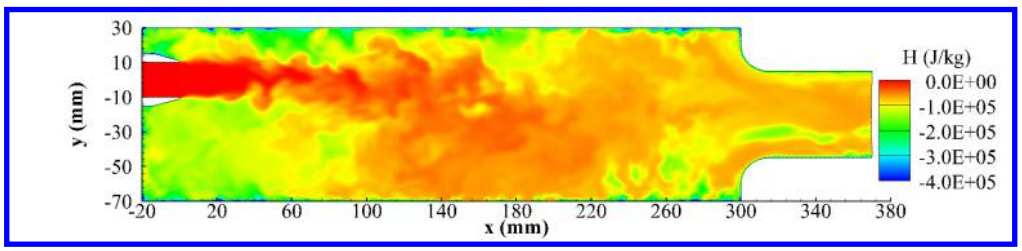

(b) case C

Figure 12. Side-view of instantaneous heat loss parameter field.

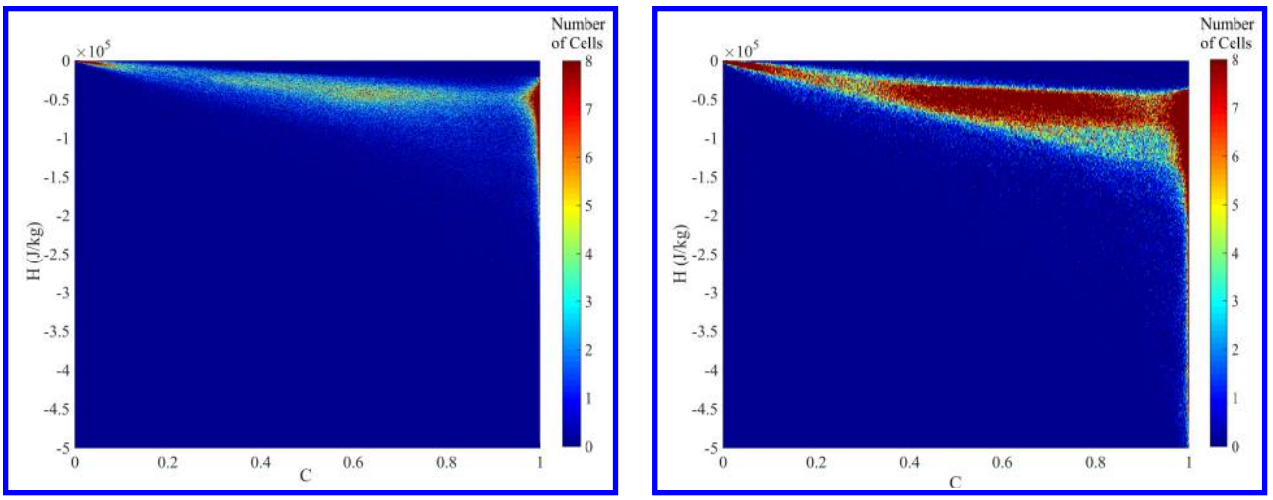

(a) case B (b) case C

Figure 13. Scatter plots of computational cells into a discretized $H - C$ space colored by number of cells within each element.

IV. Conclusions

A new non-adiabatic flamelet approach has been developed to account for heat-loss effects. A minimally-dissipative LES solver was used to simulate a realistic combustor geometry based on the DLR 3-jet experiment. It was found that the simulations predict the structure of the jet and the stabilization mechanism well, but show quantitative differences with the experiments. In particular, the jet length is underpredicted in the simulations. The effect of wall heat loss is mainly to reduce the jet core length even further, while also reducing the strength of the recirculation zones. When the wall temperature is significantly lower than the adiabatic flame temperature, the reaction zone is considerably broadened, with large sections of the domain experiencing significant heat loss.

Acknowledgments

The authors gratefully acknowledge financial support from Depart of Energy National Energy Technology Laboratory through grant DE-FE0012053. In addition, the authors thanks Dr. Ray Laster from Siemens Energy Inc. for productive discussions. The authors also thank the Texas Advanced Computing Center and the NASA High-End Computing Program through the NASA Advanced Supercomputing Division at Ames Research Center for generous allocation of computing time.

References

[1]Wunning, J. G. and GmbH, W. W., "FLOX® - Flameless Combustion," *THERMPROCESS-Symposium 2003*, 2003.

[2]Roediger, T., Lammel, O., Aigner, M., Beck, C., and Krebs, W., "Part-Load Operation of a Piloted FLOX® Combustion System," *Journal of Engineering for Gas Turbines and Power*, Vol. 135, No. 3, 2013, pp. 031503.

[3]Lammel, O., Rödiger, T., Stöhr, M., Ax, H., Kutne, P., Severin, M., Griebel, P., and Aigner, M., "Investigation of flame stabilization in a high-pressure multi-jet combustor by laser measurement techniques," *ASME Turbo Expo 2014: Turbine Technical Conference and Exposition*, American Society of Mechanical Engineers, 2014, pp. V04BT04A031–V04BT04A031.

[4]Kim, J. and Moin, P., "Application of a fractional-step method to incompressible Navier-Stokes equation," *Journal of Computational Physics*, Vol. 59, No. 2, 1984, pp. 308–323.

[5]Pierce, C. D., *Progress-variable approach for large-eddy simulation of turbulent combustion*, Ph.D. thesis, Citeseer, 2001.

[6]Akselvoll, K. and Moin, P., "Large-eddy simulation of turbulent confined coannular jets," *Journal of Fluid Mechanics*, Vol. 315, 1996, pp. 387–411.

[7]Desjardins, O., Blanquart, G., Balarac, G., and Pitsch, H., "High order conservative finite difference scheme for variable density low Mach number turbulent flows," *Journal of Computational Physics*, Vol. 227, 2008, pp. 7125–7159.

[8]Shunn, L., Ham, F., and Moin, P., "Verification of variable-density flow solvers using manufactured solutions," *Journal of Computational Physics*, Vol. 231, No. 9, 2012, pp. 3801–3827.

[9]Ham, F. and Iaccarino, G., "Energy conservation in collocated discretization schemes on unstructured meshes," *Annual Research Briefs*, Vol. 2004, 2004, pp. 3–14.

[10]Mahesh, K., Constantinescu, G., and Moin, P., "A numerical method for large-eddy simulation in complex geometries," *Journal of Computational Physics*, Vol. 197, No. 1, 2004, pp. 215–240.

[11]"The Open Source CFD Toolbox," OpenCFD Inc. http://www.openfoam.com/.

[12]Fureby, C., Chapuis, M., Fedina, E., and Karl, S., "CFD analysis of the HyShot II scramjet combustor," *Proceedings of the Combustion Institute*, Vol. 33, No. 2, 2011, pp. 2399–2405.

[13]Koo, H., Raman, V., Mueller, M., and Geigle, K. P., "Large-eddy simulation of soot formation in a model gas turbine combustor," *ASME Turbo Expo 2016*, 2016, pp. No. GT2016–57952.

[14]Lietz, C., Heye, C., Raman, V., and Blunck, D., "Flame stability analysis in an ultra compact combustor using Large Eddy Simulations," *52nd Aerospace Sciences Meeting*, No. AIAA 2014-1022, 2014.

[15]Desjardins, O., Moureau, V., and Pitsch, H., "An accurate conservative level set/ghost fluid method for simulating turbulent atomization," *Journal of Computational Physics*, Vol. 227, 2008, pp. 8395–8416.

[16]Ferziger, J. H. and Peric, M., *Computational Methods for Fluid Dynamics*, Springer, 3rd ed., 2002.

[17]Morinishi, Y., "Skew-symmetric form of convective terms and fully conservative finite difference schemes for variable density low-Mach number flows," *Journal of Computational Physics*, Vol. 229, No. 2, 2010, pp. 276–300.

[18]Issa, R. I., "Solution of the implicitly discretized fluid flow equations by operator-splitting," *Journal of computational physics*, Vol. 62, No. 1, 1986, pp. 40–65.

[19]Lietz, C., Hassanaly, M., and Raman, V., "Large eddy simulation of flame flashback in swirling premixed CH4/H2-Air flames," *The 53rd AIAA Aerospace Sciences Meeting*, American Institute of Aeronautics and Astronautics, 2015.

[20]Van Oijen, J. A. and de Goey, L. P. H., "A numerical study of confined triple flames using a flamelet-generated manifold," *Combustion Theory and Modelling*, Vol. 8, No. 1, 2004, pp. 141–163.

[21]Vreman, A., Albrecht, B., Van Oijen, J., De Goey, L., and Bastiaans, R., "Premixed and non-premixed generated manifolds in large-eddy simulation of Sandia flame D and F," *Combustion and Flame*, Vol. 153, No. 3, 2008, pp. 394–416.

[22]Pierce, C. D. and Moin, P., "Progress-variable approach for large-eddy simulation of non-premixed turbulent combustion," *Journal of Fluid Mechanics*, Vol. 504, 2004, pp. 73–97.

[23]Ottino, G., Fancello, A., Falcone, M., Bastiaans, R., and de Goey, L., "Combustion modeling Including heat loss using Flamelet Generated Manifolds: a validation study in OpenFOAM," *Flow, Turbulence and Combustion*, 2015, pp. 1–28.

[24]Fiorina, B., Baron, R., Gicquel, O., Thevenin, D., Carpentier, S., Darabiha, N., et al., "Modelling non-adiabatic partially premixed flames using flame-prolongation of ILDM," *Combustion Theory and Modelling*, Vol. 7, No. 3, 2003, pp. 449–470.

[25]Mueller, M. E. and Pitsch, H., "LES model for sooting turbulent non-premixed flames," *Combustion and Flame*, Vol. 159, No. 6, 2012, pp. 2166–2180.

[26]Access to FlameMaster. http://www.itv.rwth-aachen.de/index.php?id=128.

[27]Trisjono, P., Kleinheinz, K., Pitsch, H., and Kang, S., "Large eddy simulation of stratified and sheared flames of a premixed turbulent stratified flame burner using a flamelet model with heat loss," *Flow, Turbulence and Combustion*, Vol. 92, No. 1-2, 2014, pp. 201–235.

[28]McBride, B. J., Gordon, S., and Reno, M. A., "Coefficients for calculating thermodynamic and transport properties of individual species," *NASA Technical Memorandum 4513, NASA*, Vol. 1, 1993.

[29]Wang, C., Wen, J., Lu, S., and Guo, J., "Single-step chemistry model and transport coefficient model for hydrogen combustion," *Science China Technological Sciences*, Vol. 55, No. 8, 2012, pp. 2163–2168.

[30]Peters, N., *Turbulent Combustion*, Cambridge University Press, 2000.